

Production of π^+ and K^+ mesons in argon-nucleus interactions at 3.2 AGeV

BM@N Collaboration

S. Afanasiev¹, G. Agakishiev¹, E. Aleksandrov¹, I. Aleksandrov¹, P. Alekseev³, K. Alishina¹, E. Atkin⁶, T. Aushev⁵, V. Babkin¹, N. Balashov¹, A. Baranov², A. Baranov⁷, D. Baranov¹, N. Baranova⁷, N. Barbashina⁶, M. Baznat¹, S. Bazylev¹, M. Belov⁴, D. Blau³, G. Bogdanova⁷, D. Bogoslovsky¹, A. Bolozdynya⁶, E. Boos⁷, M. Buryakov¹, S. Buzin¹, A. Chebotov¹, J. Chen¹⁰, D. Dementev¹, A. Dmitriev¹, D. Dryablov¹, A. Dryuk⁸, P. Dulov¹, D. Egorov¹, V. Elsha¹, A. Fediunin¹, I. Filippov¹, I. Filozova¹, D. Finogeev², I. Gabdrakhmanov¹, A. Galavanov⁶, O. Gavrischuk¹, K. Gertsenberger¹, V. Golovatyuk¹, M. Golubeva², F. Guber², A. Iusupova⁸, A. Ivashkin², A. Izvestnyy², V. Kabadzhov⁹, M. Kapishin¹, I. Kapitonov¹, V. Karjavin¹, D. Karmanov⁷, N. Karpushkin², R. Kattabekov¹, V. Kekelidze¹, S. Khabarov¹, P. Kharlamov⁷, A. Khukhaeva¹, A. Khvorostukhin¹, Yu. Kiryushin¹, P. Klimai^{5,2}, D. Klimansky¹, V. Kolesnikov¹, A. Kolozhvari¹, Yu. Kopylov¹, M. Korolev⁷, L. Kovachev^{11,1}, I. Kovalev⁷, Yu. Kovalev¹, I. Kozlov⁸, V. Kozlov⁴, I. Kudryashov⁷, S. Kuklin¹, E. Kulish¹, A. Kurganov⁷, A. Kuznetsov¹, E. Ladygin¹, D. Lanskoj⁷, N. Lashmanov¹, V. Lenivenko¹, R. Lednický¹, V. Leontiev⁷, E. Litvinenko¹, Yu-G. Ma¹⁰, A. Makankin¹, A. Makhnev², A. Malakhov¹, A. Martemianov³, E. Martovitsky¹, K. Mashitsin⁸, M. Merkin⁷, S. Merts¹, A. Morozov¹, S. Morozov², Yu. Murin¹, G. Musulmanbekov¹, A. Myasnikov⁸, R. Nagdasev¹, E. Nekrasowa³, S. Nemnyugin⁸, D. Nikitin¹, S. Novozhilov¹, V. Palchik¹, I. Pelevanyuk¹, D. Peresunko³, O. Petukhov², Yu. Petukhov¹, S. Piyadin¹, M. Platonova⁷, V. Plotnikov¹, D. Podgainy¹, V. Rogov¹, I. Rufanov¹, P. Rukoyatkin¹, M. Rumyantsev¹, D. Sakulin¹, S. Sergeev¹, A. Sheremetev¹, A. Sheremeteva¹, A. Shchipunov¹, M. Shitenkov¹, M. Shopova⁹, V. Shumikhin⁶, A. Shutov¹, V. Shutov¹, I. Slepnev¹, V. Slepnev¹, I. Slepov¹, A. Solomin⁷, A. Sorin¹, V. Sosnovtsev⁶, V. Spaskov¹, A. Stavinskiy³, Yu. Stepanenko¹, E. Streletskaya¹, O. Streltsova¹, M. Strikhanov⁶, N. Sukhov¹, D. Suvarieva¹, G. Taer³, N. Tarasov¹, O. Tarasov¹, P. Teremkov⁴,

A. Terletsky¹, O. Teryaev¹, V. Tcholakov⁹, V. Tikhomirov¹, A. Timoshenko¹, N. Topilin¹, T. Tretyakova⁷, V. Tskhay⁴, E. Tsvetkov⁴, I. Tyapkin¹, V. Vasendina¹, V. Velichkov¹, V. Volkov⁷, A. Voronin⁷, A. Voronin¹, N. Voytishin¹, V. Yurevich¹, I. Yumatova², N. Zamiatin¹, M. Zavertyaev⁴, S. Zhang¹⁰, E. Zherebtsova², V. Zhezher¹, N. Zhigareva³, A. Zinchenko¹, A. Zubankov², E. Zubarev¹, M. Zuev¹

¹ Joint Institute for Nuclear Research (JINR), Dubna, Russia

² Institute for Nuclear Research of the RAS (INR RAS), Moscow, Russia

³ Kurchatov Institute, NRC, Moscow, Russia

⁴ Lebedev Physical Institute of the Russian Academy of Sciences (LPI RAS), Moscow, Russia

⁵ Moscow Institute of Physics and Technology (MIPT), Moscow, Russia

⁶ National Research Nuclear University MEPhI, Moscow, Russia

⁷ Skobeltsyn Institute of Nuclear Physics, Moscow State University (SINP MSU), Moscow, Russia

⁸ St Petersburg University (SPbU), St Petersburg, Russia

⁹ Plovdiv University “Paisii Hilendarski”, Plovdiv, Bulgaria

¹⁰ Key Laboratory of Nuclear Physics and Ion-Beam Application (MOE), Institute of Modern Physics, Fudan University, Shanghai, China

¹¹ Institute of Mechanics, Bulgarian Academy of Sciences, Sofia, Bulgaria

Abstract

First physics results of the BM@N experiment at the Nuclotron/NICA complex are presented on π^+ and K^+ meson production in interactions of an argon beam with fixed targets of C, Al, Cu, Sn and Pb at 3.2 AGeV. Transverse momentum distributions, rapidity spectra and multiplicities of π^+ and K^+ mesons are measured. The results are compared with predictions of theoretical models and with other measurements at lower energies.

1 Introduction

BM@N (Baryonic Matter at Nuclotron) is the first operational experiment at the Nuclotron/NICA accelerator complex. The Nuclotron will provide beams of a variety of particles, from protons up to gold ions, with kinetic energy in the range from 1 to 6 GeV/nucleon for light ions with Z/A ratio of ~ 0.5 and up to 4.5 GeV/nucleon for heavy ions with Z/A ratio of ~ 0.4 . At these energies, the nucleon density in the fireball created in the collisions of a heavy-ion beam with fixed targets is 3-4 times higher than the nuclear saturation density [1], thus allowing studying heavy-ion interactions in the regime of high-density baryonic matter [2].

The primary goal of the experiment, complemented by the MPD experiment that will use the Nuclotron beam in a collider mode, is to constrain the parameters of the equation of state (EoS) of high-density nuclear matter and to search for the conjectured critical end point, the onset of the deconfinement phase transition and the onset of the chiral symmetry restoration.

In addition, the Nuclotron energies are high enough to study strange mesons and (multi)-strange hyperons produced in nucleus-nucleus collisions close to the kinematic threshold [3, 4]. Studies of the excitation function of strange particle production below and near the kinematic threshold make it possible to distinguish between hard and soft behavior of the EoS [5].

In the commissioning phase, in a configuration with limited phase-space coverage, BM@N collected first experimental data with beams of carbon, argon, and krypton ions [6, 7]. This paper presents first results on π^+ and K^+ meson production in 3.2 AGeV argon-nucleus interactions.

The paper is organized as follows. Section 2 describes the experimental set-up and Section 3 is devoted to details of the event reconstruction. Section 4 describes the evaluation of the π^+ , K^+ reconstruction efficiency. Section 5 addresses the evaluation of the cross sections, multiplicities and systematic uncertainties. Experimental results on transverse momentum distributions, rapidity spectra, and multiplicities of π^+ and K^+ mesons are given in Section 6. The BM@N results are compared with predictions of theoretical models and with experimental data on medium-sized nucleus-nucleus interactions measured at lower energies. Finally, the results are summarized in Section 7.

2 Experimental set-up

The BM@N detector is a forward spectrometer covering the pseudorapidity range $1.6 \leq \eta \leq 4.4$. A schematic view of the BM@N setup in the argon-beam run is shown in Fig. 1. More details of all components of the set-up can be found in [8]. The spectrometer includes a central tracking system consisting of 3 planes of forward silicon-strip detectors (ST) and 6 planes of detectors based on gas electron multipliers (GEM) [9]. The central tracking system is located downstream of the target region inside of a dipole magnet with a bending power of about ≈ 2.1 Tm and with a gap of 1.05 m between the poles. In the measurements reported here, the central tracker covered only the upper half of the magnet acceptance.

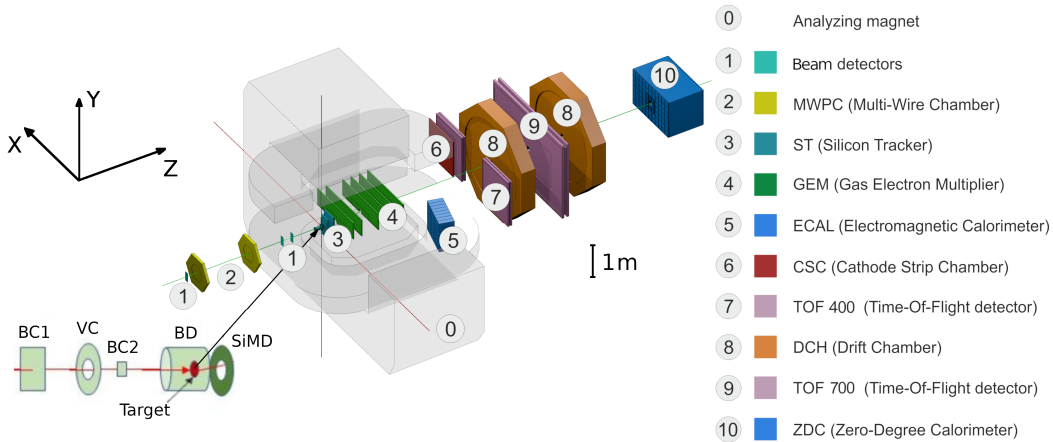


Figure 1: Schematic view of the BM@N setup in the argon beam run.

Two sets of drift chambers (DCH), a cathode strip chamber (CSC), two sets of time-of-flight detectors (ToF), and a zero-degree calorimeter (ZDC) are located downstream of the dipole magnet. The tracking system measures the momentum p of charged particles with a relative uncertainty that varies from 2.5% at a momentum of 0.5 GeV/c to 4.5% at 3.5 GeV/c as shown in Fig. 2. The time resolutions of the ToF-400 and ToF-700 systems are 84 ps and 115 ps, respectively [10].

Two beam counters (BC1, BC2), a veto counter (VC), a barrel detector (BD), and a silicon multiplicity detector (SiMD) were used for event triggering and for measurement of the incoming beam ions. The BC2 counter provided also the start time T_0 for the time of flight measurement. The BD detector consists of 40 azimuthal scintillating strips arranged around the target, and the SiMD detector consists of 60 azimuthal silicon segments situated behind the target.

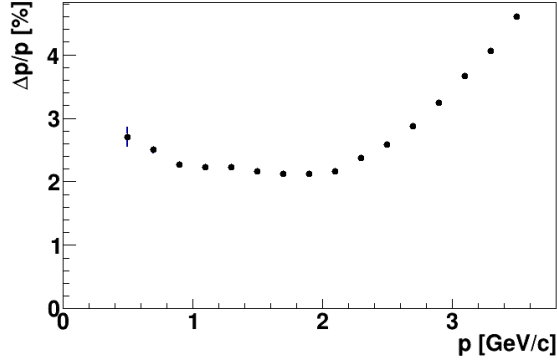


Figure 2: Relative momentum resolution as a function of the momentum.

To count the number of beam ions that passed through the target, a logical beam trigger $BT = BC1 \wedge \overline{VC} \wedge BC2$ was used. The following logic conditions were applied to generate the trigger signal: 1) $BT \wedge (BD \geq 3, 4)$; 2) $BT \wedge (SiMD \geq 3, 4)$; 3) $BT \wedge (BD \geq 2) \wedge (SiMD \geq 3)$. The trigger conditions were varied to find the optimal ratio between the event rate and the trigger efficiency for each target. Trigger condition 1 was applied for 60% of the data collected with the carbon target. This trigger fraction was continuously reduced with the atomic weight of the target down to 26% for the Pb target. The fraction of data collected with trigger condition 2 was increased from 6% for the carbon target up to 34% for the Pb target. The rest of the data were collected with trigger condition 3. The analysis presented here used the data from the forward silicon detectors, GEM detectors, outer drift chambers, cathode strip chamber, and the two sets of the time-of-flight detectors ToF-400 [11] and ToF-700 [12]. Data were collected with an argon beam intensity of a few 10^5 ions per spill and a spill duration of 2-2.5 sec. The kinetic energy of the beam was 3.2 AGeV with the spread of about 1%. A set of solid targets of various materials (C, Al, Cu, Sn, Pb) with a relative interaction length of 3% was used. The experimental data correspond to an integrated luminosity of $7.8 \mu\text{b}^{-1}$ collected with the different targets: $2.1 \mu\text{b}^{-1}$ (C), $2.3 \mu\text{b}^{-1}$ (Al), $1.8 \mu\text{b}^{-1}$ (Cu), $1.1 \mu\text{b}^{-1}$ (Sn), $0.5 \mu\text{b}^{-1}$ (Pb). A total of 16.3M argon-nucleus collisions at 3.2 AGeV were reconstructed.

3 Event reconstruction

Track reconstruction in the central tracker is based on a “cellular automaton” approach [13] implementing a constrained combinatorial search of track candidates

with their subsequent fitting by a Kalman filter to determine the track parameters. These tracks are used to reconstruct primary and secondary vertices as well as global tracks by extrapolation and matching to hits in the downstream detectors (CSC, DCH and ToF).

The primary collision vertex position (PV) is measured with a resolution of 2.4 mm in the X-Y plane perpendicular to the beam direction and 3 mm in the beam direction at the target position. The distribution of the primary vertices along the beam direction (Z_{ver}) for experimental data and Monte Carlo events is shown in Fig. 3.

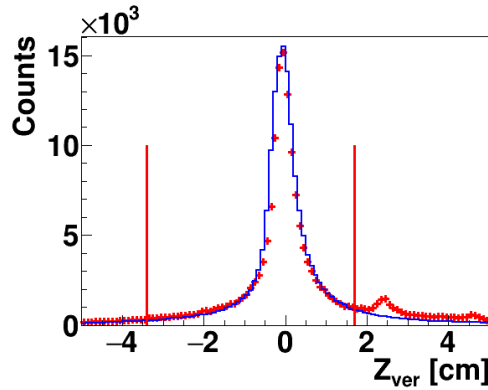


Figure 3: Distribution of the primary vertices along the Z axis for data (red crosses) and simulated events (blue histogram). The vertical lines limit the Z region accepted for the data analysis.

Charged mesons (π^+ and K^+) are identified using the time of flight Δt measured between T0 and the ToF detectors, the length of the trajectory Δl and the momentum p reconstructed in the central tracker. Then the squared mass M^2 of a particle is calculated by the formula: $M^2 = p^2((\Delta t c / \Delta l)^2 - 1)$, where c is the speed of light.

Candidates of π^+ and K^+ must originate from the primary vertex and match hits in the CSC and ToF-400 or in the DCH and ToF-700 detectors. The following criteria are required for selecting π^+ and K^+ meson candidates:

- Each track has at least 4 hits in the GEM detectors (6 detectors in total) [9]. Hits in the forward silicon detectors are used to reconstruct the track, but no requirements are applied to the number of hits;
- Tracks originate from the primary vertex. The deviation of the reconstructed vertex from the target position along the beam direction is limited to -3.4

cm $< Z_{\text{ver}} - Z_0 < 1.7$ cm, where Z_0 is the target position. The upper limit corresponds to $\sim 5.7\sigma$ of the Z_{ver} spread and cuts off interactions with the trigger detector located 3 cm behind the target (see Fig. 3). The two vertical lines in the figure limit the region of the Z coordinates accepted for the data analysis for all the targets. The beam interaction rate with the trigger detector is well below 1% and was not simulated since it does not affect the precision in Monte Carlo simulation.

- Distance from a track to the primary vertex in the X-Y plane at Z_{ver} (DCA) is required to be less than 1 cm, which corresponds to 4σ of the vertex resolution in the X-Y plane;
- Momentum range of positively charged particles $p > 0.5$ GeV/c and $p > 0.7$ GeV/c is limited by the acceptance of the ToF-400 and ToF-700 detectors, respectively;
- Distance of extrapolated tracks to the CSC (DCH) hits as well as to the ToF-400 (ToF-700) hits should be within $\pm 2.5\sigma$ of the momentum dependent hit-track residual distributions as shown in Fig. 4 for the ToF-400 system.

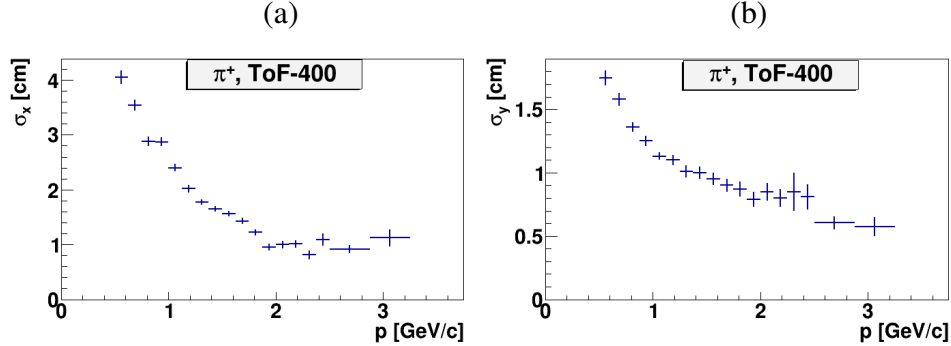


Figure 4: σ_x (a) and σ_y (b) of the Gaussian fit of the ToF-400 hit residuals with respect to positively charged pions depending on the particle momentum.

The spectra of the mass squared (M^2) of positively charged particles produced in interactions of the 3.2 AGeV argon beam with various targets are shown in Figs. 5a and 5b for ToF-400 and ToF-700 data, respectively. The π^+ and K^+ signals are extracted in the M^2 windows from -0.09 to 0.13 $(\text{GeV}/c^2)^2$ and from 0.18 to 0.32 $(\text{GeV}/c^2)^2$, respectively. The signals of π^+ and K^+ and their statistical errors are calculated according to the formulae: $sig = hist - bg$,

$err_{stat} = \sqrt{hist + bg}$, assuming the background uncertainty is \sqrt{bg} . Here $hist$ and bg denote the histogram and background integral yields within the selected M^2 windows.

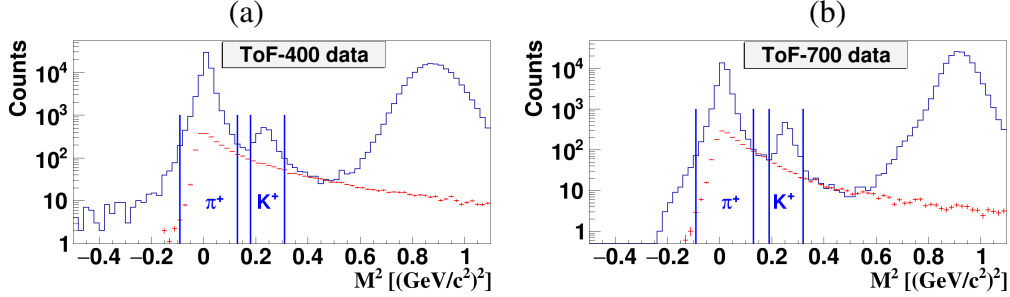


Figure 5: M^2 spectra of positively charged particles produced in argon-nucleus interactions and measured in the ToF-400 (a) and ToF-700 (b) detectors. The vertical lines show the ranges of selected π^+ and K^+ mesons. The red points show the background estimated from “mixed events”.

The shape of the background under the π^+ and K^+ signals in the M^2 spectra is estimated using the “mixed event” method. For that, tracks reconstructed in the central tracker are matched to hits in the ToF detectors taken from different events. The “mixed event” background is normalized to the integral of the signal histogram outside the M^2 windows of π^+ and K^+ mesons, i.e in the M^2 ranges 0.13-0.18 $(\text{GeV}/c^2)^2$ and 0.32-0.4 $(\text{GeV}/c^2)^2$. It was found that the background level differs for light and heavy targets and for different intervals of rapidity and transverse momentum.

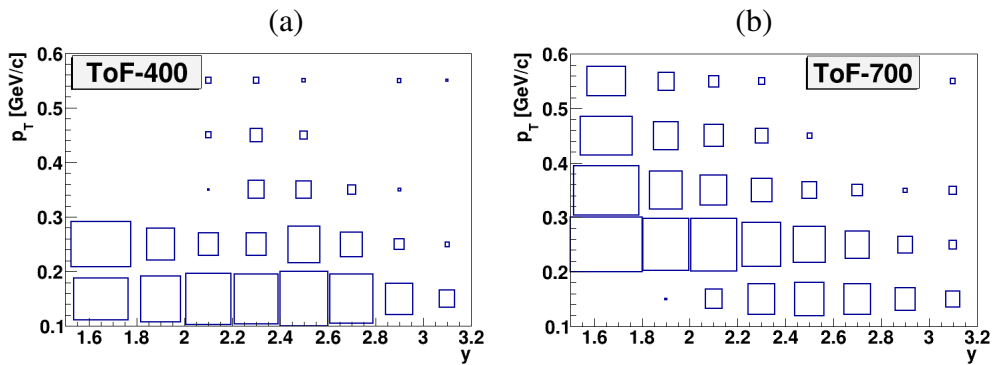


Figure 6: Distribution of the π^+ signals measured in ToF-400 (a) and ToF-700 (b) in the rapidity and transverse momentum bins in Ar+Sn interactions.

The ToF-400 and ToF-700 detectors cover different ranges of rapidity and

transverse momentum of detected particles. Fig. 6 shows the signals of π^+ mesons measured in ToF-400 and ToF-700 in the rapidity vs transverse momentum plane in Ar+Sn interactions before making corrections for the efficiency.

4 Reconstruction efficiency and trigger performance

To evaluate the π^+ and K^+ reconstruction efficiency, Monte Carlo data samples of argon-nucleus collisions were produced with the DCM-SMM event generator [14, 15]. Propagation of particles through the entire detector volume and responses of the detectors were simulated using the GEANT3 program [16] integrated into the BmnRoot software framework [17]. To properly describe the GEM detector response in the magnetic field, the Garfield++ toolkit [18] for simulation of the micropattern gaseous detectors was used.

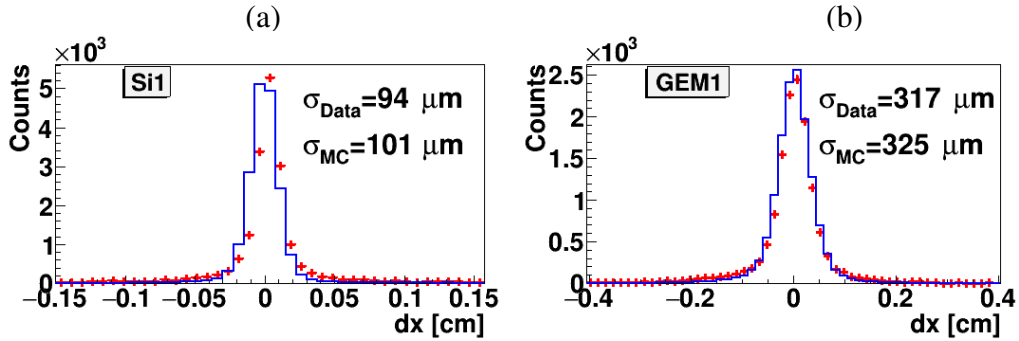


Figure 7: Residual distributions of hits in the X projection (magnet deflection plane) with respect to reconstructed tracks: (a) - in the first forward silicon plane, (b) - in the first GEM plane. The experimental data are shown as red crosses, and the simulated data are shown as blue histograms.

The efficiencies of the forward silicon, GEM, CSC, DCH and ToF detectors were adjusted during simulation in accordance with the measured detector efficiencies. The Monte Carlo events went through the same chain of reconstruction and identification as the experimental events.

The level of agreement between the Monte Carlo and experimental distributions is demonstrated on a set of observables: primary vertices distribution along the Z-axis (Fig. 3), residuals in the central tracker detectors (Fig. 7), closest distance from a track to the primary vertex in the X-Y plane (DCA), χ^2/NDF , number of reconstructed tracks at the primary vertex and number of hits per track

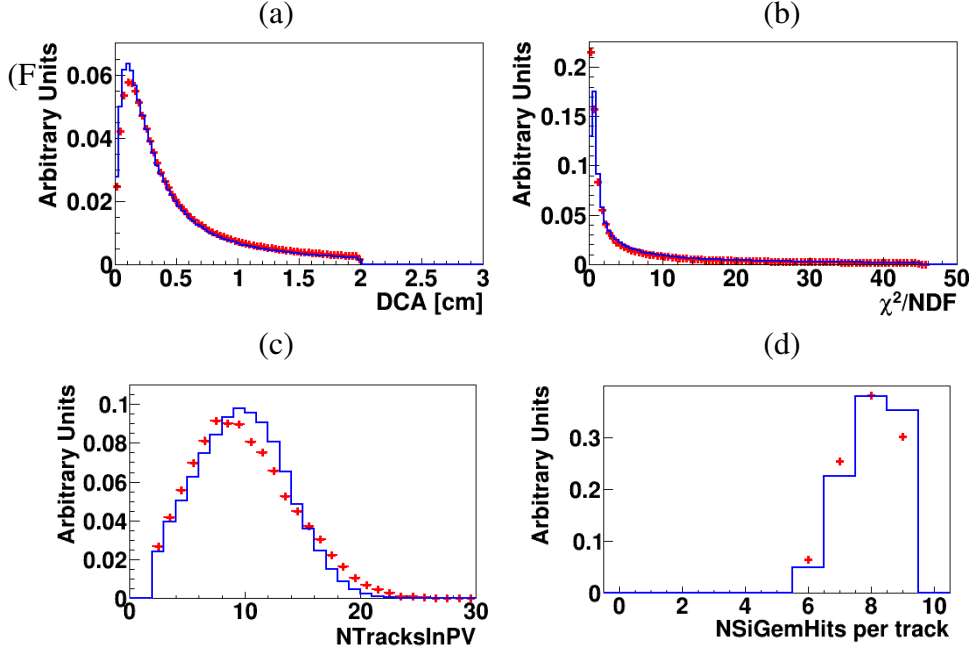


Figure 8: Comparison of experimental distributions (red crosses) and GEANT distributions of events generated with the DCM-SMM model (blue lines), in Ar+A collisions at 3.2 AGeV: (a) DCA, distance of closest approach to the primary vertex; (b) χ^2/NDF of reconstructed tracks; (c) number of reconstructed tracks in the primary vertex in Ar+Cu interactions; (d) Hits per track in the 3 forward Si and 6 GEM detectors.

The π^+ and K^+ reconstruction efficiencies are calculated in intervals of rapidity y and transverse momentum p_T . The reconstruction efficiency includes the geometrical acceptance, the detector efficiency, the kinematic and spatial cuts, the loss of π^+ and K^+ due to in-flight decays and the meson reconstruction. The reconstruction efficiencies of π^+ detected in ToF-400 and ToF-700 are shown in Fig. 9 as function of y (left panel) and p_T (right panel) for Ar+Sn interactions.

The trigger efficiency ϵ_{trig} depends on the number of fired channels in the BD (SiMD) detectors. It was calculated for events with reconstructed π^+ and K^+ mesons using event samples recorded with an independent trigger based on the SiMD (BD) detectors. The BD and SiMD detectors cover different and non-overlapping regions of the BM@N acceptance, that is, they detect different collision products. For the BD trigger efficiency estimation, the following relation is used: $\epsilon_{trig}(\text{BD} \geq m) = N(\text{BD} \geq m \wedge \text{SiMD} \geq n)/N(\text{SiMD} \geq n)$, where m and n are the minimum number of fired channels in BD ($m = 3, 4$) and SiMD ($n = 3, 4$) (see Section 2). A similar relation is used to evaluate the SiMD trigger

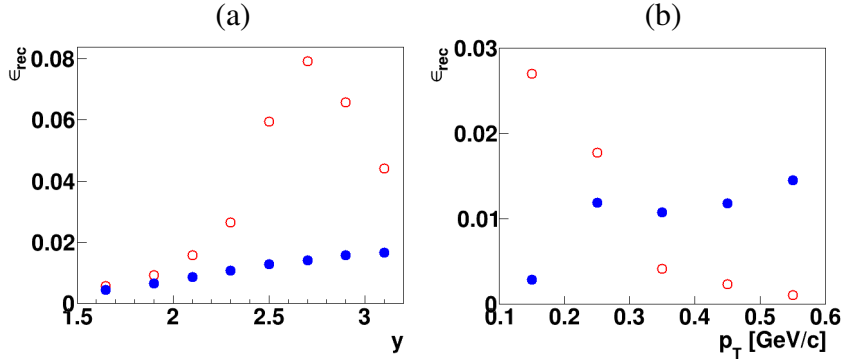


Figure 9: Reconstruction efficiency of π^+ produced in Ar+Sn collisions, detected in ToF-400 (open red circles) and ToF-700 (full blue circles) as function of rapidity y (a) and p_T (b). The efficiency includes both acceptance and reconstruction.

efficiency. The BD (SiMD) trigger efficiency is averaged over all data with the different values of the minimum number of fired channels in SiMD (BD).

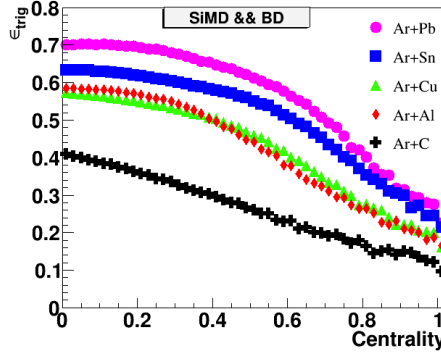


Figure 10: Trigger efficiency for interactions of the argon beam with various targets (C, Al, Cu, Sn, Pb) with a reconstructed π^+ as a function of the event centrality estimated from the simulation.

The efficiency of the combined BD and SiMD triggers was calculated as the product of the efficiencies of the BD and SiMD triggers. The trigger efficiency, for events with a reconstructed π^+ , averaged over all data collected with the trigger conditions 1) $\text{BT} \wedge (\text{BD} \geq 3, 4)$; 2) $\text{BT} \wedge (\text{SiMD} \geq 3, 4)$; 3) $\text{BT} \wedge (\text{BD} \geq 2) \wedge (\text{SiMD} \geq 3)$ (see Section 2) is shown in Fig. 10 as a function of the event centrality estimated from simulation. The event centrality is determined as the fraction of the interaction cross section in the interval $[0, b]$ of the impact parameter b of the

nucleus-nucleus collision to the total interaction cross section. It is clearly seen that the trigger efficiency decreases with a decrease in the mass of the target and an increase in the centrality of the collision. The trigger efficiency for events with a reconstructed K^+ was found to be slightly higher, 6% higher in Ar+C collisions and 11% higher for Ar+Pb collisions for the combined trigger $BT \wedge (BD \geq 2) \wedge (SiMD \geq 3)$.

5 Cross sections, multiplicities, and systematic uncertainties

The π^+ (K^+) mesons in Ar+C, Al, Cu, Sn, Pb interactions are measured in the following kinematic range: transverse momentum $0.1 < p_T < 0.6$ GeV/c ($0.1 < p_T < 0.5$ GeV/c) and rapidity in the laboratory frame $1.5 < y < 3.2$ ($1.0 < y < 2.0$). The analysis takes into account the track dependence of the trigger efficiency. No significant variation in the reconstruction efficiency with the track multiplicity was found. The differential cross sections $d^2\sigma_{\pi,K}(y, p_T)/dydp_T$ and multiplicities $d^2N_{\pi,K}(y, p_T)/dydp_T$ of π^+ and K^+ meson production in Ar+C, Al, Cu, Sn, Pb interactions are calculated using the relations:

$$\begin{aligned} d^2\sigma_{\pi,K}(y, p_T)/dydp_T &= \Sigma[d^2n_{\pi,K}(y, p_T, N_{tr})/(\epsilon_{trig}(N_{tr})dydp_T)] \times 1/(L\epsilon_{rec}(y, p_T)) \\ d^2N_{\pi,K}(y, p_T)/dydp_T &= d^2\sigma_{\pi,K}(y, p_T)/(\sigma_{inel}dydp_T) \end{aligned} \quad (1)$$

where the sum is performed over bins of the number of tracks in the primary vertex, N_{tr} , $n_{\pi,K}(y, p_T, N_{tr})$ is the number of reconstructed π^+ or K^+ mesons in the intervals dy and dp_T , $\epsilon_{trig}(N_{tr})$ is the track-dependent trigger efficiency, ϵ_{rec} is the reconstruction efficiency of π^+ or K^+ , L is the luminosity, and σ_{inel} is the inelastic cross section for argon-nucleus interactions.

Table 1 summarizes the mean values, averaged over p_T , y , and N_{tr} , of the systematic uncertainties of the various factors of Eq. (1), $n_{\pi,K}$, ϵ_{rec} , and ϵ_{trig} . Details are given below, including the uncertainty of the luminosity measurement. The model uncertainty of σ_{inel} is given in Table 3.

Several sources are considered for the evaluation of the systematic uncertainty of the π^+ and K^+ yield, $n_{\pi,K}$, and the reconstruction efficiency ϵ_{rec} . The most significant ones are discussed below. Some of them affect both the yield $n_{\pi,K}$ and the reconstruction efficiency, ϵ_{rec} . For these cases the correlated effect is taken into account by the variations on the $n_{\pi,K}/\epsilon_{rec}$ ratio:

- Systematic uncertainty of the central tracking detector efficiency: it is estimated from the remaining difference in the number of track hits in the

central detectors in the simulation relative to the data (see Fig. 8d) and found to be within 3%.

- Systematic uncertainty of the matching of central tracks to the CSC (DCH) hits and ToF-400 (ToF-700) hits: it is estimated from the remaining difference in the matching efficiency in the simulation relative to the data and found to be within 5%.
- Systematic uncertainty of the reconstruction efficiency due to the remaining difference in the X/Y distribution of primary vertices in the simulation relative to the data.
- Systematic uncertainty of the background subtraction in the mass-squared M^2 spectra of identified particles: it is estimated as the difference between the background integral under the meson windows taken from “mixed events” (as described in Section 3) and from the fitting of the M^2 spectra by a linear function. The latter is done in the M^2 range $-0.14-0.4$ $(\text{GeV}/c^2)^2$, excluding the π^+ and K^+ windows.

The total systematic uncertainty of the yield and reconstruction efficiency for the various targets, calculated as the quadratic sum of these uncertainties, is listed in Table 1.

The luminosity is calculated from the beam flux Φ as given by the beam trigger (see Section 2) and the target thickness l using the relation: $L = \Phi\rho l$ where ρ is the target density expressed in atoms/cm³. The systematic uncertainty of the luminosity is estimated from the fraction of the beam which can miss the target, determined from the vertex positions, and found to be within 2%.

Table 1: Mean systematic uncertainties in y , p_T bins of the π^+ and K^+ mesons measured in argon-nucleus interactions (see text for details).

	Ar+C %	Ar+Al %	Ar+Cu %	Ar+Sn %	Ar+Pb %
π^+					
n_π, ϵ_{rec}	14	12	12	10	10
ϵ_{trig}	9	7	7	7	7
Total	17	14	14	13	13
K^+					
n_K, ϵ_{rec}	25	23	14	13	15
ϵ_{trig}	31	14	9	8	8
Total	40	27	17	16	17

For the evaluation of the systematic uncertainty of the trigger efficiency ϵ_{trig} , the following sources are considered:

- The systematic uncertainty associated with the factorization assumption of the two trigger factors, BD and SiMD, was estimated from the difference of ϵ_{trig} evaluated as described in Section 4, with the result evaluated using the limited amount of events registered with the beam trigger BT.
- To estimate a possible distortion of ϵ_{trig} ($BD \geq m$) due to the selection of events with the hardware-set condition $N(SiMD \geq n)$, ϵ_{trig} was also evaluated using the events recorded with the beam trigger BT. The difference between the results is treated as another source of systematic uncertainty of the trigger efficiency.
- Variations of the trigger efficiency on the track multiplicity in the primary vertex and on the X/Y vertex position.

The total systematic uncertainty of the trigger efficiency for the various targets, calculated as the quadratic sum of these uncertainties, is listed in Table 1.

The inelastic cross sections of Ar+C, Al, Cu, Sn, Pb interactions are taken from the predictions of the DCM-SMM model which are consistent with the results calculated by the formula: $\sigma_{inel} = \pi R_0^2 (A_P^{1/3} + A_T^{1/3})^2$, where $R_0 = 1.2$ fm is the effective nucleon radius, A_P and A_T are the atomic numbers of the projectile and target nucleus [19]. The systematic uncertainties for the Ar+C, Al, Cu, Sn, Pb inelastic cross sections are estimated from an alternative formula [20] which approximates the measured nucleus-nucleus cross sections: $\sigma_{inel} = \pi R_0^2 (A_P^{1/3} + A_T^{1/3} - b)^2$ with $R_0 = 1.46$ fm and $b = 1.21$. The values and uncertainties of σ_{inel} for Ar+C, Al, Cu, Sn, Pb interactions are given in Table 3.

6 Results and discussion

The rapidity spectra of π^+ and K^+ mesons are shown in Figs. 11 and 12, respectively, for different p_T bins for various targets. At a kinetic energy of 3.2 GeV/nucleon, the rapidity of the nucleon-nucleon center-of-mass (CM) system is $y_{CM} = 1.08$. The rapidity intervals covered in the present measurements, $y = 1.5 - 3.2$ and $y = 1.0 - 2.0$ for π^+ and K^+ , respectively, correspond therefore to the forward and central rapidity regions in the nucleon-nucleon CM system. Figs. 11 and 12 show also a comparison of the experimental results with the predictions of the DCM-SMM [14, 15], UrQMD [21] and PHSD [22] models. For π^+ , the three models have quite similar predictions, in particular at medium and high p_T bins for all targets, except for the C target (and to a lesser extent also the

Al target) where the PHSD model is markedly different from the DCM-SMM and UrQMD models at mid-rapidity. The three models are in reasonable agreement with the experimental results at forward rapidity and high p_T for all targets. In general, for the heavier targets, the models overshoot the data at mid-rapidity and high- p_T , the UrQMD predictions being closer to the data. All three models fail to reproduce the shape and magnitude of the C data at mid-rapidity. For K^+ , there are large differences, up to a factor of ~ 2 , between the three models. In general, the PHSD and DCM-SMM models over-predict the data for all p_T bins, whereas the UrQMD is closer to the data.

The p_T spectra of π^+ and K^+ mesons are shown in Figs. 13 and 14, respectively, for different rapidity y bins and for all targets. Due to the low statistics of the K^+ yield in Ar+C interactions, the results are shown only for the entire measured ranges of y and p_T .

The p_T spectra of K^+ mesons integrated over the entire measured rapidity range are shown in Fig. 15. In Figs. 13 – 15, the p_T spectra are parameterised by an exponential function as:

$$1/p_T \cdot d^2N/dydp_T \propto \exp(-(m_T - m_{\pi,K})/T_0),$$

where $m_T = \sqrt{m_{\pi,K}^2 + p_T^2}$ is the transverse mass, and the inverse slope, T_0 , is a fitting parameter. The T_0 values obtained from the fits of the π^+ spectra are shown in Fig. 16. The T_0 values are about 40 MeV at the most forward rapidity $y \approx 3$, rising to 90 MeV toward more central rapidities at $y \approx 1.6$. In general, the y dependence of the fitting results for π^+ mesons is consistent with the predictions of the DCM-SMM, UrQMD and PHSD models, but the experimental results exhibit a flatter dependence of the T_0 values in the central rapidity range as opposed to the rising dependence of the inverse slopes predicted by the models.

The T_0 values for K^+ mesons obtained in 3 y bins are shown in Fig. 17. In spite of the large statistical and systematic errors, T_0 exhibits a rather weak dependence on y . The T_0 values for the entire measured range of $1.0 < y < 2.0$ are consistent, within the experimental uncertainties, with 80 MeV for all the targets (see Table 2). The weak dependence of T_0 on y is reproduced by the PHSD and DCM-SMM models, the latter being in general closer to the data. The UrQMD predicts a strong dependence on y , with T_0 values much larger than the measured ones.

The measured π^+ and K^+ meson multiplicities are extrapolated to the entire kinematic range using the averaged extrapolation factors obtained from the predictions of the DCM-SMM, UrQMD and PHSD models shown in Table 3. The largest difference of the extrapolation factors from their average value is taken as

Table 2: π^+ and K^+ meson multiplicities measured in Ar+C, Al, Cu, Sn, Pb interactions at the argon beam energy of 3.2 AGeV. The first error is statistical, the second one is systematic. The third error, given for the full π^+ and K^+ multiplicities, is the model uncertainty in the extrapolation factor to the full phase space (see text and Table 3).

3.2 AGeV argon beam	Ar+C	Ar+Al	Ar+Cu	Ar+Sn	Ar+Pb
Measured π^+ mult. N_{π^+}	$0.42 \pm 0.008 \pm 0.045$	$1.00 \pm 0.01 \pm 0.07$	$1.14 \pm 0.01 \pm 0.08$	$1.28 \pm 0.01 \pm 0.09$	$1.25 \pm 0.01 \pm 0.08$
Measured K^+ mult. $N_{K^+}/10^{-2}$	$1.59 \pm 0.29 \pm 0.65$	$3.90 \pm 0.28 \pm 0.61$	$4.17 \pm 0.21 \pm 0.66$	$5.60 \pm 0.22 \pm 0.75$	$5.10 \pm 0.22 \pm 0.92$
Full π^+ mult. $N_{\pi^+}^{tot}$	$1.365 \pm 0.026 \pm 0.146 \pm 0.08$	$3.73 \pm 0.04 \pm 0.26 \pm 0.13$	$5.07 \pm 0.04 \pm 0.36 \pm 0.08$	$6.55 \pm 0.05 \pm 0.46 \pm 0.33$	$7.39 \pm 0.06 \pm 0.47 \pm 0.69$
Full K^+ mult. $N_{K^+}^{tot}/10^{-2}$	$4.47 \pm 0.81 \pm 1.83 \pm 1.05$	$11.8 \pm 0.9 \pm 1.8 \pm 2.6$	$13.9 \pm 0.7 \pm 2.2 \pm 2.7$	$20.7 \pm 0.8 \pm 2.8 \pm 3.3$	$20.9 \pm 0.9 \pm 3.8 \pm 2.2$
$N_{K^+}/N_{\pi^+}/10^{-2}$ Measured range	$3.79 \pm 0.69 \pm 1.52$	$3.90 \pm 0.28 \pm 0.55$	$3.66 \pm 0.19 \pm 0.53$	$4.39 \pm 0.18 \pm 0.51$	$4.11 \pm 0.18 \pm 0.68$
$N_{K^+}^{tot}/N_{\pi^+}^{tot}/10^{-2}$, Full kin. range	$3.27 \pm 0.6 \pm 1.38 \pm 0.79$	$3.16 \pm 0.23 \pm 0.54 \pm 0.71$	$2.75 \pm 0.14 \pm 0.48 \pm 0.54$	$3.16 \pm 0.13 \pm 0.48 \pm 0.52$	$2.83 \pm 0.12 \pm 0.54 \pm 0.39$
K^+ inv. slope T_0 , MeV, Meas. range	$67 \pm 12 \pm 12$	$80 \pm 7 \pm 5$	$81 \pm 5 \pm 5$	$81 \pm 5 \pm 4$	$78 \pm 5 \pm 4$

systematic uncertainty of the extrapolation factor.

Table 3: Extrapolation factors for π^+ and K^+ multiplicities, from the measured range to the entire kinematical range, obtained as an average of the extrapolation factors derived from the DCM-SMM, PHSD, and UrQMD models. The maximum difference between the model factors from their averaged value is taken as the uncertainty of the extrapolation factors. A_{part} is the number of participant nucleons obtained from the DCM-SMM model. σ_{inel} is the inclusive cross section for inelastic Ar+A interactions.

	Ar+C	Ar+Al	Ar+Cu	Ar+Sn	Ar+Pb
π^+ Extrap. factor	3.25 ± 0.18	3.73 ± 0.13	4.45 ± 0.07	5.12 ± 0.26	5.91 ± 0.55
K^+ Extrap. factor	2.81 ± 0.66	3.02 ± 0.67	3.34 ± 0.65	3.7 ± 0.58	4.1 ± 0.43
$A_{\text{part, DCM-SMM}}$	14.8	23.0	33.6	48.3	63.6
$\sigma_{\text{inel, mb [19]}}$	1470 ± 50	1860 ± 50	2480 ± 50	3140 ± 50	3940 ± 50

The multiplicities of K^+ and π^+ mesons and their ratios are summarized in Table 2. The K^+ to π^+ ratios do not show a significant dependence on the mean number of participant nucleons A_{part} , determined as the mean number of nucleons that underwent at least one inelastic collision. The values of A_{part} , based on the DCM-SMM model, are listed in Table 3.

The π^+ and K^+ multiplicities per participant nucleon, A_{part} , are plotted and compared to predictions of the DCM-SMM, UrQMD and PHSD models in Figs. 18. For π^+ , the three models predict a steady decrease of this ratio with increasing atomic weight of the target, from C to Pb. This behavior is observed in the data with all targets with the exception of the C target. A similar trend is also observed in the data for ratios of the K^+ multiplicities to A_{part} . The K^+ to π^+ multiplicity ratios are shown in Fig. 18c. They show no dependence on the number of participant nucleons contrary to the three models that show a small increase. The PHSD model exhibits a rather small increase and, within the experimental uncertainties, is compatible with the measured K^+ to π^+ multiplicity ratios.

The π^+ and K^+ meson multiplicities in argon-nucleus interactions can be compared with previously published results. The HADES experiment measured

Ar+KCl interactions at the lower beam kinetic energy of 1.76 AGeV [23–25]. The total π^- and K^+ multiplicities in semi-central events (with an average number of participant nucleons A_{part} of 38.5) was reported to be 3.9 and $2.8 \cdot 10^{-2}$, respectively. The results presented here for Ar+Cu interactions at the beam kinetic energy of 3.2 AGeV (A_{part} of 33.6, see Table 3) are higher by factors of 1.3 and 5 relative to the HADES results. The difference in the K^+ multiplicities could be explained by the energy dependence of the K^+ cross section near the kinematic threshold for K^+ production ($E_{\text{thr}}(NN) \sim 1.58$ GeV). The effective inverse slope parameters obtained by HADES from the m_T spectra of π^- and K^+ extrapolated to $y^* = 0$ are 82.4 MeV and 89 MeV, respectively, comparable to those reported here (see Figs. 16 and 17).

The FOPI experiment measured Ni+Ni interactions at the beam kinetic energy of 1.93 AGeV [26–28]. Consistent results were also reported by the KaoS experiment that measured the K^+ multiplicities in Ni+Ni interactions at kinetic energies of 1.5 and 1.93 AGeV [29, 30]. The total K^+ multiplicity in semi-central and central Ni+Ni interactions, with A_{part} of 46.5 and 75, were reported to be $3.6 \cdot 10^{-2}$ and $8.25 \cdot 10^{-2}$, respectively. These values can be compared with the results reported here in Table 2 for the various targets. The K^+/π^+ multiplicity ratio measured by FOPI in triggered semi-central events is $7.6 \cdot 10^{-3}$, which is by a factor ~ 4 smaller than the K^+/π^+ multiplicity ratio obtained here in Ar + Sn interactions for the entire kinematical range (A_{part} of 48.3, see Table 3). It should be taken into account that the beam kinetic energy of the FOPI experiment (1.93 AGeV) is lower than that of the BM@N experiment. The effective inverse slope of 110.9 MeV, estimated by FOPI at $y^* = 0$ from the K^+ transverse mass spectrum is consistent within uncertainties with the inverse slope parameter T_0 , reported here for K^+ in the range $y^* \gtrsim 0$ (see Fig. 17). The consistency of the inverse slope parameters reported here with the results of the HADES and FOPI experiments indicates the absence of a strong dependence of T_0 on the beam energy and atomic weight of the colliding nuclei.

The total pion multiplicity N_{π}^{tot} , where $N_{\pi}^{\text{tot}} = N_{\pi^+}^{\text{tot}} + N_{\pi^-}^{\text{tot}} + N_{\pi^0}^{\text{tot}}$, normalized to the average number of participant nucleons A_{part} are compiled in Fig. 19 for different collision systems and beam energies. References [31] and [32] contain a compilation of pion data for interactions of nucleon-nucleon (N+N) [33], Mg+Mg [34], La+La [35], Au+Au [36–38], Ar+KCl [39], Si+Al, S+S [40, 41], Pb+Pb [42, 43], Au+Au [44–47]. To estimate N_{π}^{tot} from the π^+ multiplicities reported here, the predictions of the DCM-SMM model are used. The total K^+ multiplicity in the entire kinematic range normalized to the average number of participant nucleons A_{part} are compiled in Fig. 20. The figure includes the world

data taken from [26,43,48–50] together with the results reported here. Figures 19 and 20 demonstrate that the BM@N results reported here are consistent with the world data on the production of π and K^+ mesons.

7 Summary

First physics results of the BM@N experiment are presented on the π^+ and K^+ meson yields and their ratios in argon-nucleus interactions at the beam kinetic energy of 3.2 AGeV. The results are compared with the DCM-SMM, UrQMD and PHSD models and with the previously published results of other experiments.

The inverse slope parameter T_0 of the π^+ transverse momentum spectrum is about 40 MeV in the forward rapidity range, rising to 90 MeV in the central rapidity range. In general, the y-dependence of T_0 is consistent with the predictions of the models, but there is a tendency for the experimental results to show a flatter dependence of the slope values in the central rapidity range compared to a rising dependence predicted by the models.

The T_0 value for K^+ exhibits a weak dependence on the rapidity. The PHSD and DCM-SMM models reproduce the weak dependence of T_0 , whereas UrQMD predicts much larger T_0 values.

The ratios of the K^+ to π^+ multiplicities show no significant dependence on the mean number of participant nucleons A_{part} in argon-nucleus collisions. The PHSD prediction is compatible with this result, whereas the DCM-SMM and UrQMD models predict a smooth rising of the K^+ to π^+ ratio with A_{part} .

The π and K^+ multiplicities normalized to A_{part} are found to be consistent with the rising energy dependence of the world data on the production of π and K^+ mesons measured for various colliding nuclei and beam energies.

Acknowledgments. The BM@N Collaboration acknowledges the efforts of the staff of the accelerator division of the Laboratory of High Energy Physics at JINR that made this experiment possible, I.Tserruya and V.Pozdniakov for fruitful discussions of the analysis and results. The BM@N Collaboration acknowledges support of the HybriLIT of JINR, HPC Village project and HGPU group for the provided computational resources.

References

- [1] B. Friman, W. Nörenberg, and V.D. Toneev, Eur. Phys. J. A 3 (1998).
- [2] J. Randrup and J. Cleymans, Phys. Rev. C 74 (2006) 047901.
- [3] NICA White Paper, Eur. Phys. J. A 52 (2016).
- [4] BM@N Conceptual Design Report: http://nica.jinr.ru/files/BM@N/BMN_CDR.pdf
- [5] Ch. Fuchs, Prog. Part. Nucl. Phys. 56 (2006) 1-103.
- [6] M. Kapishin (for the BM@N Collaboration), Nucl. Phys. A 982 (2019) 967-970.
- [7] M. Kapishin (for the BM@N Collaboration), SQM 2019 proceedings, 285 Springer Proc. Phys. 250 (2020) 21-27.
- [8] BM@N project:
http://nica.jinr.ru/files/BM@N/BMN_project.pdf
- [9] D. Baranov et al., JINST 12 (2017) no. 06, C06041
- [10] K. Alishina et al., Phys. Part. Nucl., 53 (2022) no. 2, 470-475.
- [11] V. Babkin et al., Nucl. Instrum. Meth. A 824, P.490-492 (2016); V. Babkin et al., Proceedings of Science, 2014, Vol.213 (Proceedings of TIPP-2014), P.289.
- [12] N. Kuzmin et al., Nucl. Instrum. Meth. A 916, P. 190-194 (2019).
- [13] V. Akishina and I. Kisel, J. Phys.: Conf. Ser. 599, 012024 (2015), I. Kisel, Nucl. Instrum. Meth. A 566, 85 (2006).
- [14] N. Amelin, K. Gudima, and V. Toneev, Sov. J. Nucl. Phys. 51, 1093 (1990).
- [15] M. Baznat, A. Botvina, G. Musulmanbekov, V. Toneev, V. Zhezher, Phys. Part. Nucl. Lett. 17 (2020) no. 3; arXiv: 1912.09277v.
- [16] CERN Program Library, Long Writeup W5013, Geneva, CERN, 1993.
- [17] <https://git.jinr.ru/nica/bmnroot>

- [18] <http://garfieldpp.web.cern.ch/garfieldpp>
- [19] K. Kanaki, PhD Thesis, Technische Universität Dresden, 2007.
- [20] H. Angelov et al., P1-80-473, JINR, Dubna.
- [21] S. A. Bass et al., Prog. Part. Nucl. Phys. 41 225 (1998).
- [22] W. Cassing and E. L. Bratkovskaya, Nucl. Phys. A 831 (2009) 215-242.
- [23] G. Agakishiev et al., HADES Collaboration, Eur. Phys. J. A 47 (2011) 21.
- [24] G. Agakishiev et al., HADES Collaboration, Phys. Rev. C 80 (2009) 025209.
- [25] G. Agakishiev et al., HADES Collaboration, Phys. Rev. C 82 (2010) 044907.
- [26] D. Best et al., FOPI Collaboration, Nucl. Phys. A 625 (1997) 307-324.
- [27] N. Bastid et al., FOPI Collaboration, Phys. Rev. C 76 (2007) 024906.
- [28] K. Piasecki et al., FOPI Collaboration, Phys. Rev. C 99 (2019) 1, 014904.
- [29] M. Menzel et al., KaoS Collaboration, Phys. Lett. B 495 (2000) 26-32.
- [30] A. Forster et al., KaoS Collaboration, Phys. Rev. C 75 (2007) 024906.
- [31] P. Senger et al., J. Phys. G 25 (1999) R59-R131.
- [32] J. Adamczewski-Musch et al., Eur. Phys. J. A 56 (2020) 259.
- [33] Gazdzicki M. and Röhlich D., 1995 Z. Phys. C 65 215.
- [34] Anikina et al., JINR Rapid Comm Dubna, 1 (1989) 12.
- [35] Harris J. W. et al., 1987 Phys. Rev. Lett. 58 463.
- [36] Pelte D. et al., 1997 Z. Phys. A 357 215.
- [37] Wagner A. et al., 1998 Phys. Lett. B 420 20.
- [38] Schwalb O. et al., 1994 Phys. Lett. B 321 20.
- [39] Harris J. W. et al., 1985 Phys. Lett. B 153 377.
- [40] T. Abbott et al. (E-802 Collaboration), Phys. Rev. C 50 (1993) 1024.

- [41] J. Bachler et al., Phys. Rev. Lett. 72 (1994) 1419.
- [42] Jacobs P. and NA49 Collaboration 1997 Proc. of the 3rd Int. Conf. on the Physics and Astrophysics of the Quark Gluon Plasma (Jaipur, India) (Delhi: Narosa).
- [43] Afanasiev S. V. et al., Phys. Rev. C. 66 054902 (2002).
- [44] W. Reisdorf et al. (FOPI Collaboration), Nucl. Phys. A 781, 459 (2007).
- [45] A.R. Wolf et al. (TAPS Collaboration), Phys. Rev. Lett. 80, 5281 (1998).
- [46] R. Averbeck et al., Phys. Rev. C 67, 024903 (2003).
- [47] J.L. Klay et al. (E895 Collaboration), Phys. Rev. C 68, 054905 (2003).
- [48] R. Barth et al. Phys. Rev. Lett. 78 (1997), p. 4007.
- [49] L. Ahle et al. (E802 Collaboration), Phys. Rev. C 60, 044904 (1999).
- [50] L. Ahle et al. (E802 Collaboration), Phys. Rev. C 58, 3523 (1998).

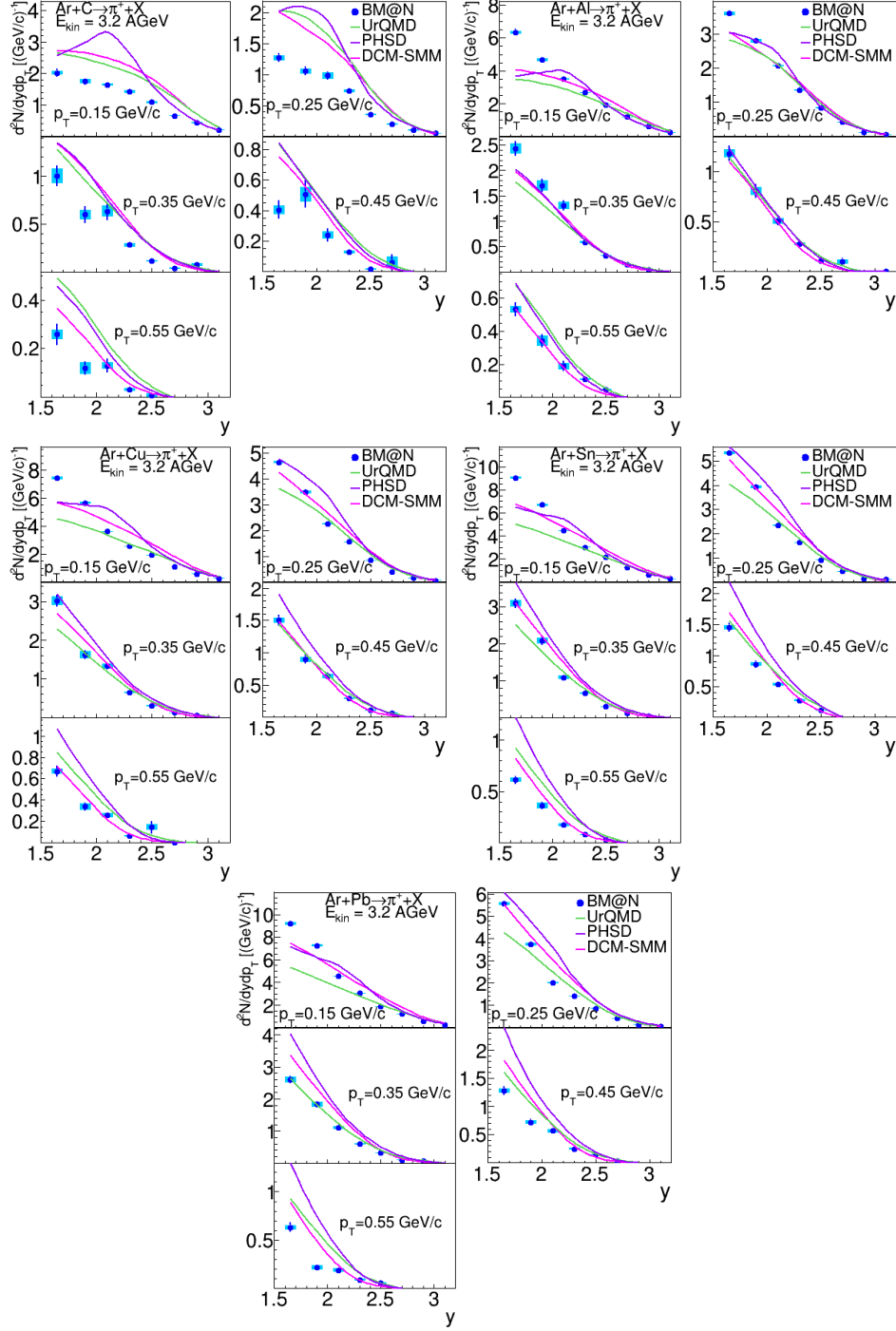


Figure 11: Rapidity spectra (y) of π^+ mesons produced in Ar+C, Al, Cu, Sn, Pb interactions at a kinetic energy of 3.2 AGeV. The results are presented for different p_T bins. The vertical bars and boxes represent the statistical and systematic uncertainties, respectively. The predictions of the DCM-SMM, UrQMD and PHSD models are shown as rose, green and magenta lines.

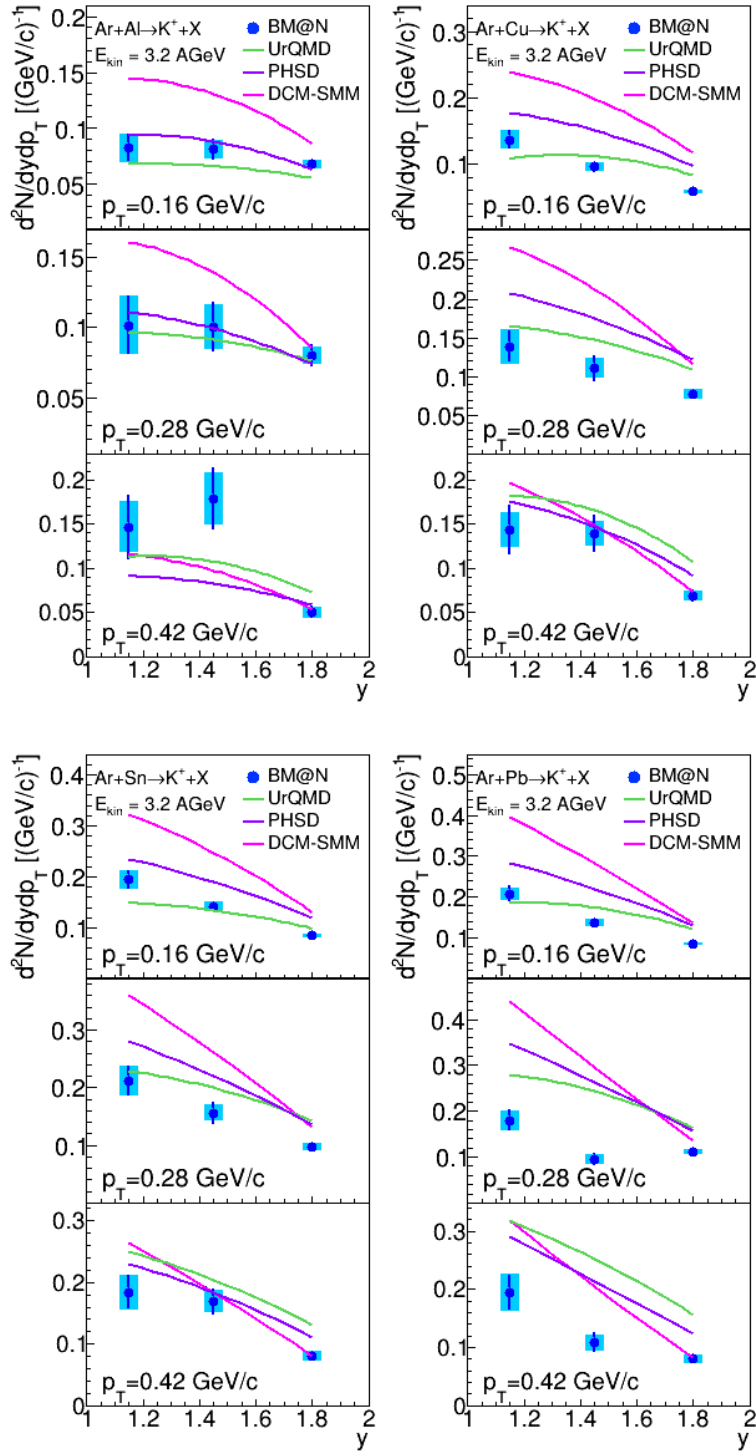


Figure 12: Rapidity spectra (y) of K^+ mesons produced in Ar+Al, Cu, Sn, Pb interactions at a kinetic energy of 3.2 AGeV. The results are presented for different p_T bins. The vertical bars and boxes represent the statistical and systematic uncertainties, respectively. The predictions of the DCM-SMM, UrQMD and PHSD models are shown as rose, green and magenta lines.

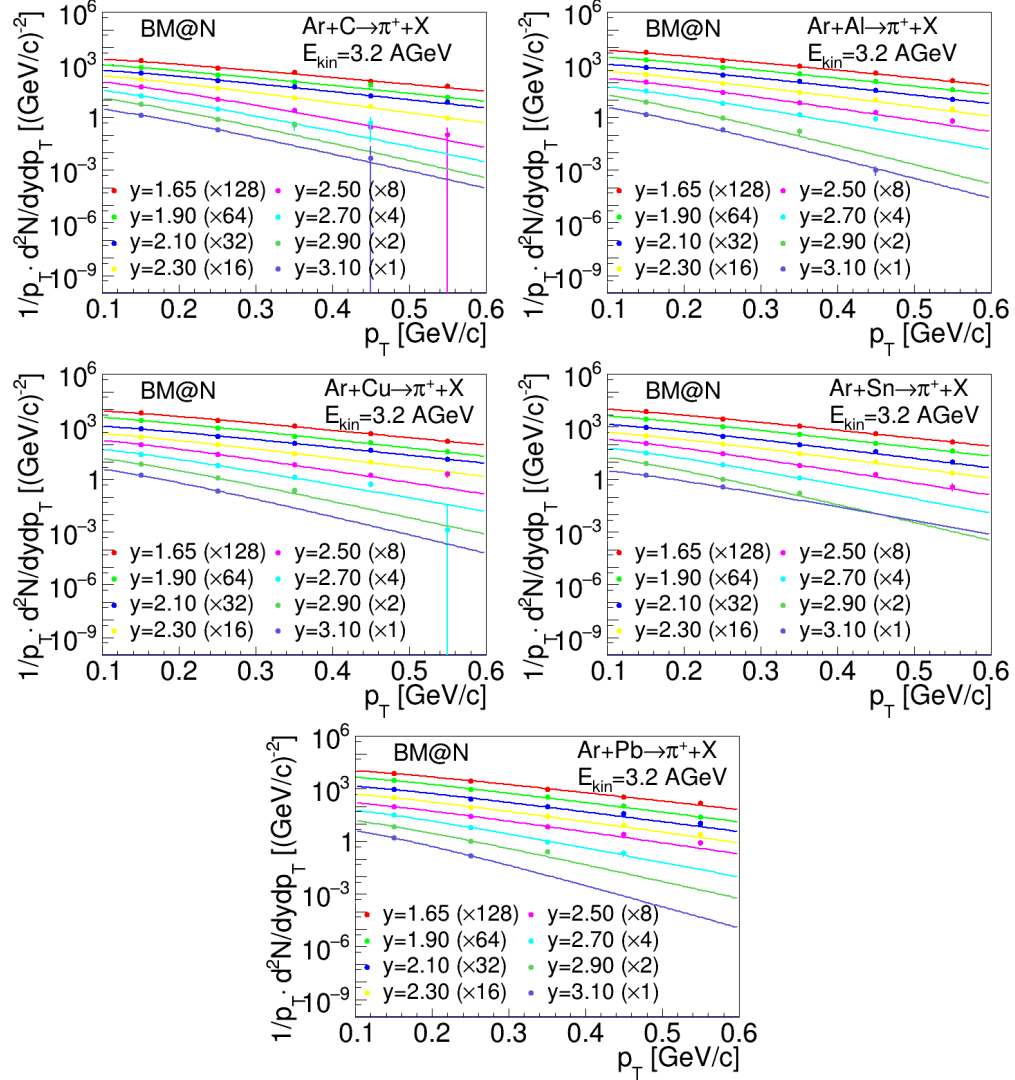


Figure 13: Transverse momentum (p_T) spectra of π^+ mesons produced in Ar+C, Al, Cu, Sn, Pb interactions at 3.2 AGeV. The results are given for bins of the π^+ rapidity. The lines represent the results of the parametrization described in the text.

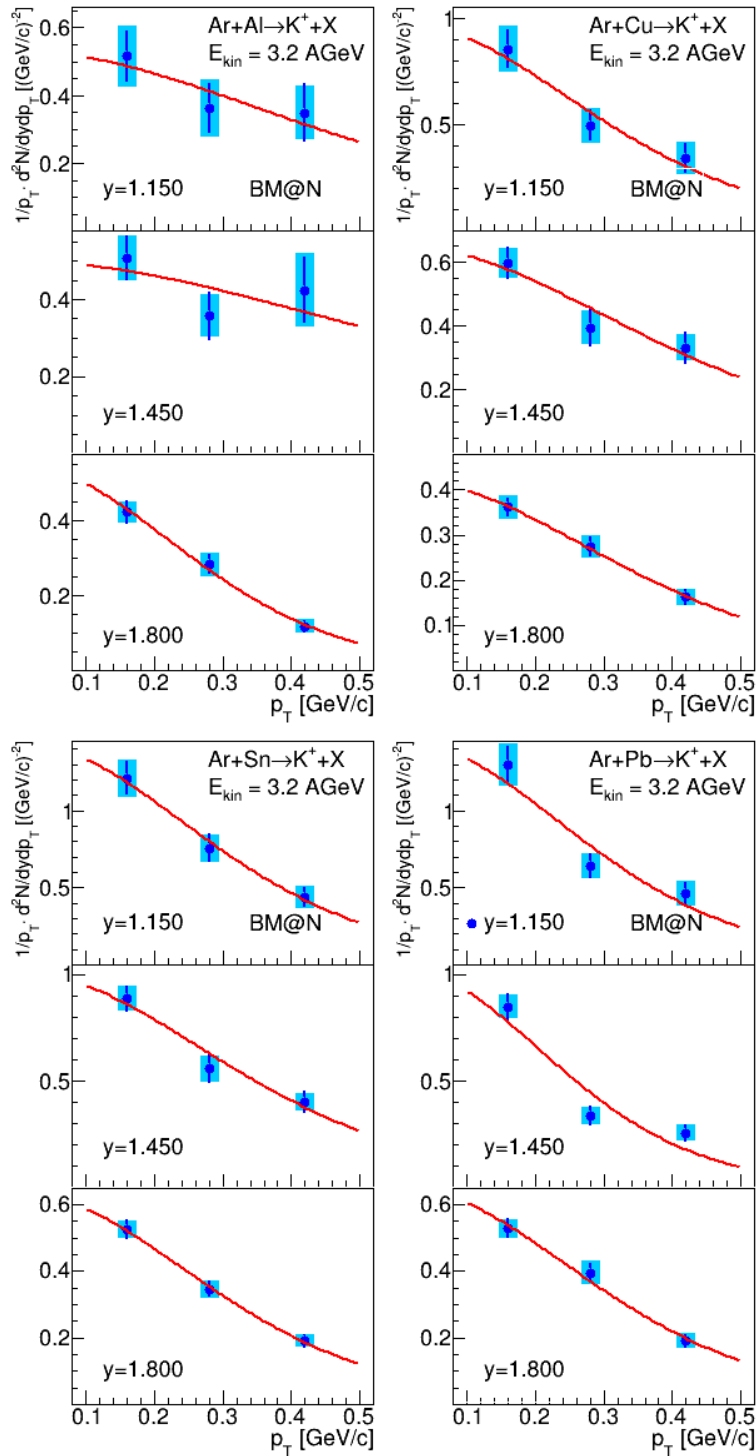


Figure 14: Transverse momentum (p_T) spectra of K^+ mesons produced in Ar+Al, Cu, Sn, Pb interactions at 3.2 AGeV. The results are given for three bins of the K^+ rapidity. The vertical bars and boxes represent the statistical and systematic uncertainties, respectively. The lines represent the results of the parametrization described in the text.

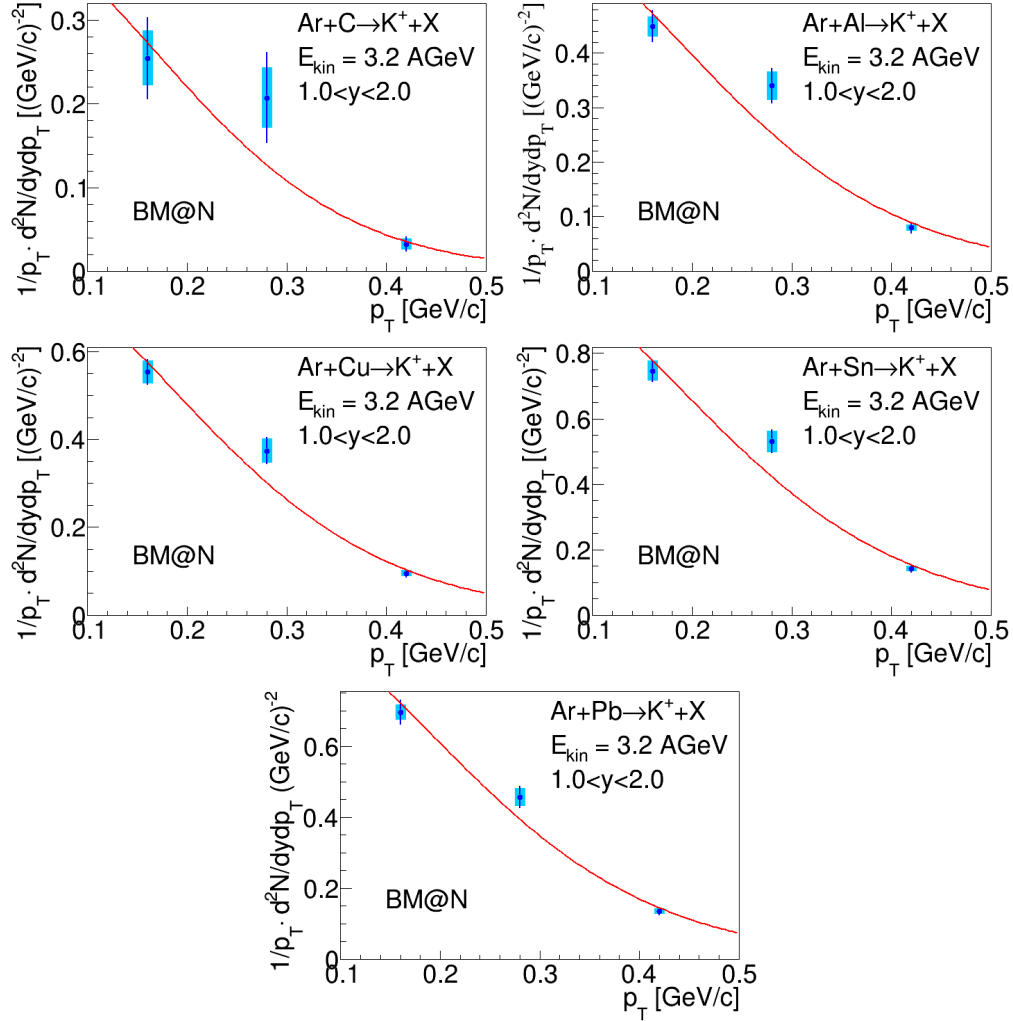


Figure 15: Transverse momentum (p_T) spectra of K^+ mesons produced in Ar+C, Al, Cu, Sn, Pb interactions at 3.2 AGeV for the entire measured K^+ rapidity range. The vertical bars and boxes represent the statistical and systematic uncertainties, respectively. The lines represent the results of the parametrization described in the text.

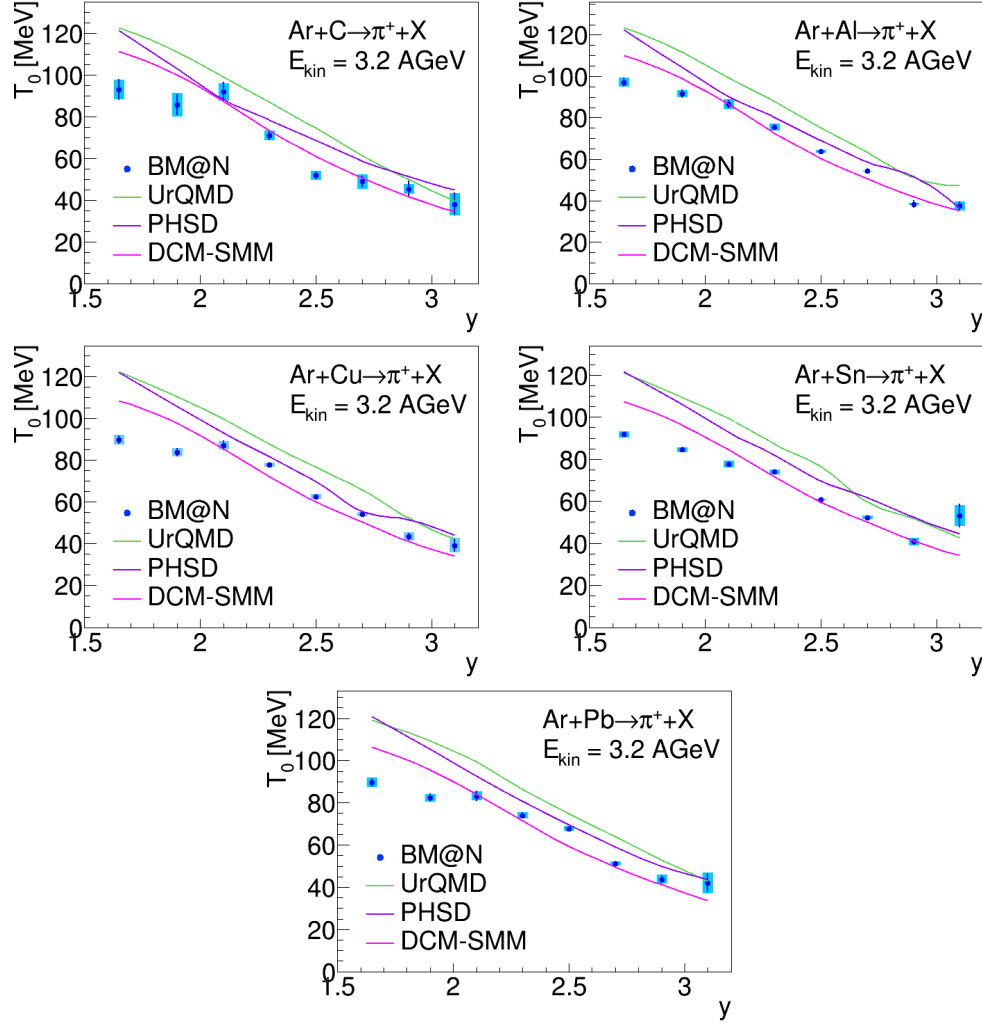


Figure 16: Rapidity y dependence of the inverse slope parameter T_0 determined from the fits of the π^+ p_T spectra in Ar+C, Al, Cu, Sn, Pb interactions. The vertical bars and boxes represent the statistical and systematic uncertainties, respectively. The predictions of the DCM-SMM, UrQMD and PHSD models are shown as rose, green and magenta lines.

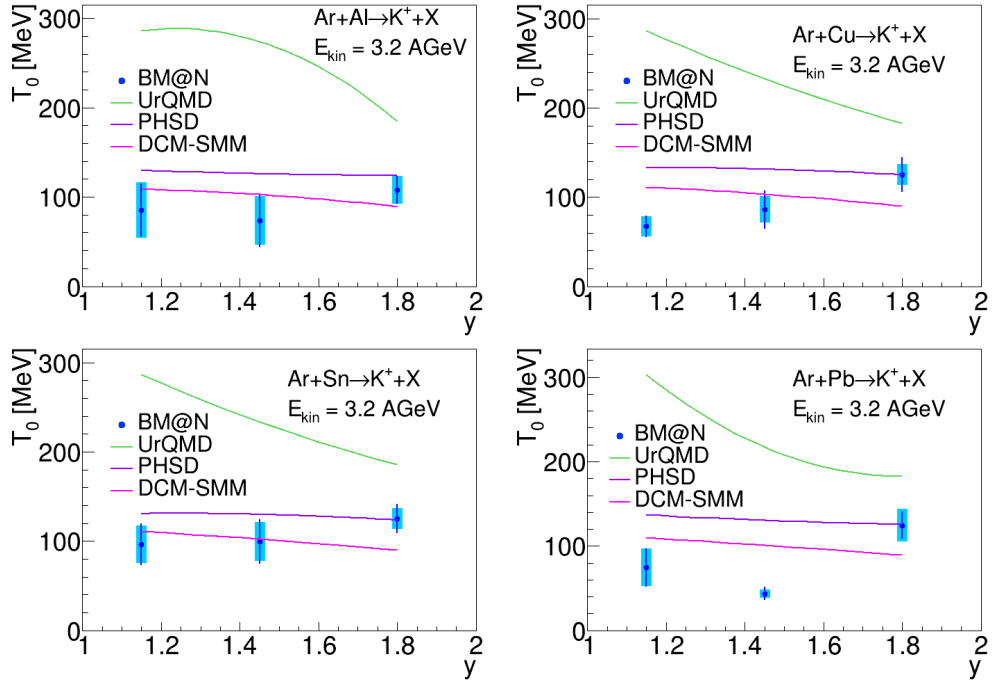


Figure 17: Rapidity y dependence of the inverse slope parameter T_0 extracted from the fits of the K^+ p_T spectra in Ar+Al, Cu, Sn, Pb interactions. The vertical bars and boxes represent the statistical and systematic uncertainties, respectively. The predictions of the DCM-SMM, UrQMD and PHSD models are shown as rose, green and magenta lines.

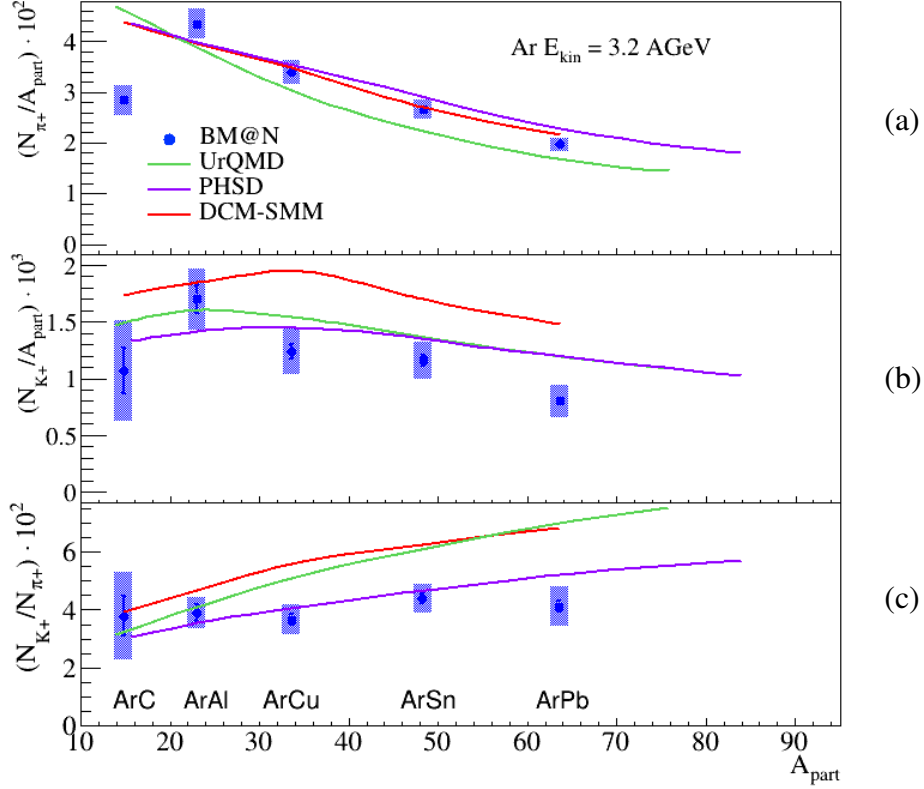


Figure 18: Ratios of the π^+ (a) and K^+ (b) multiplicities to the number of participant nucleons and ratios of the K^+ to π^+ multiplicities (c) in the measured kinematic range in Ar+C, Al, Cu, Sn, Pb interactions. The vertical bars and boxes represent the statistical and systematic uncertainties, respectively. The results are compared with predictions of the DCM-QGSM, UrQMD and PHSD models for argon-nucleus interactions shown as red, green, and magenta lines.

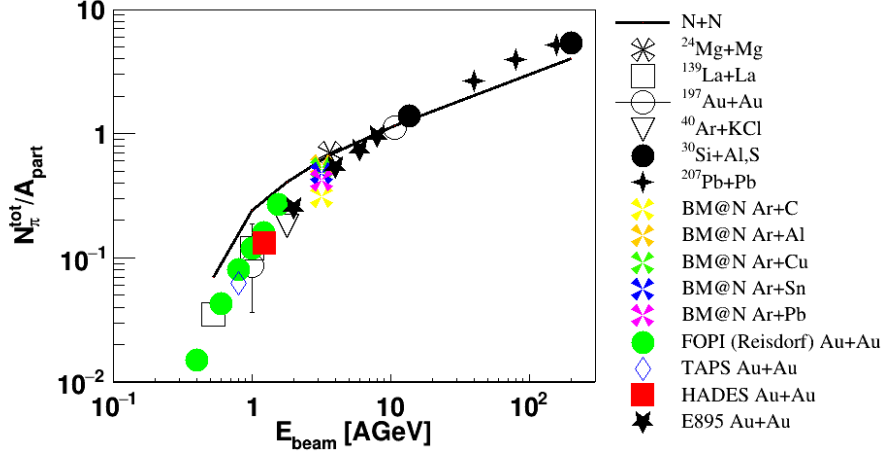


Figure 19: Comparison of the BM@N results to the world measurements (references in the text) of the total pion multiplicity N_{π}^{tot} per participant nucleon A_{part} as a function of the beam kinetic energy E_{beam} .

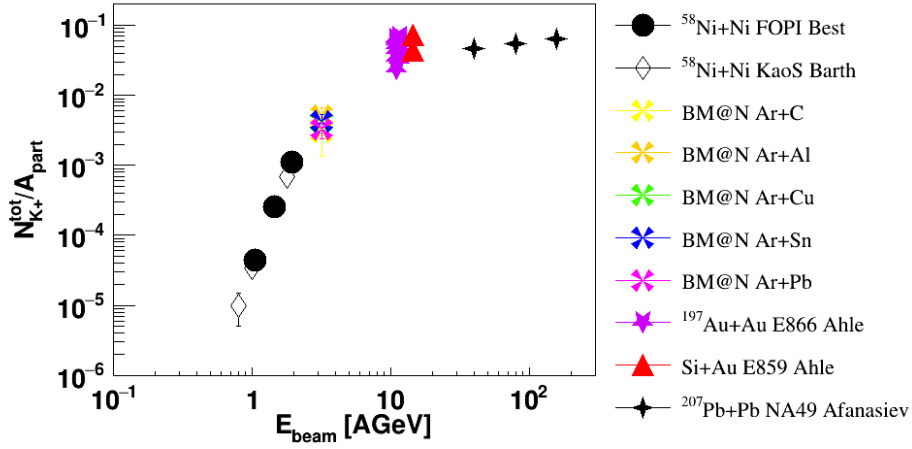


Figure 20: Comparison of the BM@N results to the world measurements (references in the text) of the K^+ multiplicity per participant nucleon A_{part} as a function of the beam kinetic energy E_{beam} .